Determination of the Rate of Dissipation of Turbulent Energy from Simultaneous Temperature and Velocity Shear Microstructure Measurements

N. S. OAKEY

Atlantic Oceanographic Laboratory, Bedford Institute of Oceanography, Dartmouth, Nova Scotia, Canada,[1] *and Applied Physics Laboratory, University of Washington, Seattle 98105*

(Manuscript received 20 July 1981, in final form 22 December 1981)

ABSTRACT

Spectra of turbulence have been examined for both temperature gradient and velocity shear. The data for this comparison are 10–15 m segments of vertical microstructure profiles (at depths of 5–100 m) obtained during the 1978 Joint Air Sea Interaction experiment (JASIN). From the simultaneous measurement of these two microstructure quantities, the universal spectral constant q (the least principal rate of strain of the velocity spectrum) has been determined to be 3.7 ± 1.5. As well, the dissipation rate has been calculated from the high-wavenumber cut-off of the temperature microstructure spectra (ϵ_B) and from velocity shear (ϵ_{SH}). For a range of values from 8×10^{-9} to 5×10^{-7} m^2 s^{-3} these two measures, ϵ_B and ϵ_{SH}, agree to within a factor of 2 on average. And finally, estimates of χ_θ (temperature dissipation rate), ϵ and mean temperature gradient have been used to estimate a mixing efficiency, $\Gamma = 0.24$.

1. Introduction

Many recent papers have described measurements of either temperature microstructure or velocity microstructure. These papers have examined the questions of mixing and turbulence from measured velocity shear on the one hand, and from the resultant signature of temperature gradients on the other hand. Very little has been reported on simultaneous measurement of these quantities. It is the purpose of this paper to examine several vertical microstructure profiles in which both velocity shear and temperature gradient variance are well resolved and measured simultaneously by sensors separated by only a few centimeters.

It will be necessary as a framework for later discussions to present some of the formulas derived from turbulence theory. A detailed description of the universal spectral forms for isotropic velocity turbulence is given in the Appendix. A brief summary is given here. The reciprocal of the Kolmogoroff length scale is defined here to be a viscous cutoff wavenumber k_s, in cyclic units,

$$k_s = (\epsilon\nu^{-3})^{1/4} \quad [\mathrm{m}^{-1}], \tag{1.1}$$

where ϵ is the turbulent energy dissipation per unit mass and ν the kinematic viscosity. In the present study the cyclic wavenumber $\hat{k}$ [m^{-1}] is used throughout where $\hat{k} = k/2\pi$ (k is the radian wavenumber). A universal spectrum of velocity shear [Eq. (A9)], $\theta(\hat{k})$, is defined by

$$\theta(\hat{k}) = k_s^2(\epsilon\nu^5)^{1/4} G_2(\hat{k}/k_s) \quad [\mathrm{s}^{-2}\,(\mathrm{cpm})^{-1}]. \tag{1.2}$$

The universal nondimensional spectrum is defined in the Appendix and numerical values are given in Table A1. These values of $G_2(\hat{k}/k_s)$ are derived from data of Nasmyth (1970, personal communication). Eq. (1.2) expresses the hypothesis that the amplitude versus wavenumber of the isotropic velocity-shear spectrum is determined solely by the rate at which energy cascades from larger to smaller scales and is dissipated at a rate ϵ.

The dissipation rate is determined from the velocity-shear spectrum by integration and (including factors for isotropy) is given by

$$\epsilon = \frac{15}{2}\nu\overline{\left(\frac{\partial u'}{\partial z}\right)^2} \quad [\mathrm{m}^2\,\mathrm{s}^{-3}]. \tag{1.3}$$

In this expression $\overline{(\partial u'/dz)^2}$ is the variance in the vertical gradient of turbulent fluctuations in the x direction (z down). We could also have used $\overline{(\partial v'/dz)^2}$.

For a scalar (temperature) in a turbulent field the spectrum of gradient fluctuations in one dimension can be represented by the Batchelor (1959) form. This can be written (for cyclic wavenumbers) as

$$S(\hat{k}) = \left(\frac{q}{2}\right)^{1/2} \frac{\chi_\theta}{k_B D}\, g(q, \hat{k}/k_B) \quad [^\circ\mathrm{C}^2\,\mathrm{m}^{-2}\,(\mathrm{cpm})^{-1}], \tag{1.4}$$

where $\hat{k}$ is the cyclic wavenumber as defined above.

[1] Present affiliation.

0022-3670/82/030256-16$08.00

The reciprocal of the Batchelor length scale is defined here to be a diffusive cutoff wavenumber

$$k_B = (\epsilon/\nu D^2)^{1/4} \quad [\mathrm{m}^{-1}], \tag{1.5}$$

expressed in cyclic units, where ν and D are respectively the viscosity and thermal diffusivity; q is a universal constant related to the least principal rate of strain of the velocity spectrum and χ_θ is a temperature dissipation rate defined by

$$\chi_\theta = 6D \int_0^\infty S(\hat{k})d\hat{k} = 6D\overline{\left(\frac{\partial T'}{\partial z}\right)^2} \quad [^\circ\mathrm{C}^2\ \mathrm{s}^{-1}], \tag{1.6}$$

where T' is the temperature fluctuation. The universal nondimensional spectral form $g(q, \hat{k}/k_B)$ is given by

$$g(q, \hat{k}/k_B) = 2\pi\left[\exp(-\alpha^2/2) - \alpha\int_\alpha^\infty \exp(-x^2/2)dx\right], \tag{1.7}$$

where

$$\alpha = (2q)^{1/2}(2\pi\hat{k}/k_B). \tag{1.8}$$

The universal constant q has been estimated by Grant *et al.* (1968) as 3.9 ± 1.5. Gibson (1968) argues theoretically that $3^{1/2} < q < 2(3^{1/2})$.

The stated purpose of this paper can now be readily defined in terms of the previous formulas. It is: 1) to determine experimentally the value of q and 2) to compare the dissipation rate of turbulent energy as determined directly from velocity shear to that determined indirectly from the temperature-gradient data.

To accomplish 1), the value of ϵ from (1.3) is used to calculate k_B; χ_θ is determined from (1.6). Plotting measured temperature-gradient data in normalized form, $S_m(\hat{k})/(\chi_\theta/k_B D)$, as a function of $\hat{k}/k_B$ allows one to find the value of q which gives the best fit of the normalized data to the assumed universal form $(\frac{1}{2}q)^{1/2}g(q, \hat{k}/k_B)$.

The alternate (and equivalent) analysis of purpose 2) is akin to the method of Dillon and Caldwell (1980) and Caldwell *et al.* (1980) wherein the turbulent dissipation is determined from well-resolved temperature-gradient spectra. Using a fixed value of q (in this case a value of $q = 4$ was selected) the "best-fit" of the Batchelor spectrum to the high-wavenumber portion of the temperature-gradient spectrum is found. This yields the cutoff wavenumber k_B, from which one can calculate a dissipation rate ϵ_B using Eq. (1.5). These values will be compared to those determined simultaneously from velocity shear, ϵ_{SH}, using Eq. (1.3).

2. Instrumentation

The data for the present discussion were obtained using the microstructure profiler OCTUPROBE II (OCeanic TUrbulence PROBE). This instrument (Oakey, 1977; Oakey and Elliott, 1982) consists of a cylinder 0.15 m in diameter and 1.6 m long containing electronics and recording components with forward stings containing preamps and supporting a variety of microstructure sensors. The vehicle is ballasted and drag-stabilized to free-fall at a nominal speed of 0.5–0.6 m s^{-1}. It is recovered and redeployed using a light, nearly neutrally buoyant tether line. Using this tethered free-fall method one can easily obtain five or six vertical profiles of microstructure to a depth of 100 m during the recording limit of 25 min set by the tape recorder. Data are recorded internally in multiplexed FM (IRIG) format on a miniature reel-to-reel NAGRA SN tape recorder. It is replayed upon recovery of OCTUPROBE for display, editing and analog-to-digital conversion using conventional FM-FM telemetry techniques.

During every vertical profile, signals are recorded from temperature-gradient microstructure and two perpendicular components of horizontal velocity-shear microstructure and, as well, pressure and temperature signals. Temperature gradient is obtained using a DISA model 55R46 thin-film thermometer. It is used in a transformer-coupled ac bridge which has a nominal sensitivity of 5°C V^{-1} with a nonlinearity of ±0.1°C. The noise at the bridge output is equivalent to 2×10^{-4} °C over the bandwidth of 1–100 Hz. The frequency response of the thin-film thermometer is limited by the boundary layer. The equivalent time constant is obtained by examining the probe's response to a heated plume at various speeds using the method described by Fabula (1968). At the profiling speeds used for OCTUPROBE the thin-film thermometer has an equivalent time constant of ~2 m s, which means that probe frequency-response corrections are smaller than they would be for thermistors. On the other hand, the signal-to-noise ratio for these two devices heavily favors thermistors. Horizontal velocity shear is measured using a probe designed originally by Siddon (1971) for use in air and later adapted by Osborn and Siddon (1975) for use in water; it has been described in several recent articles (Osborn and Crawford, 1980; Osborn, 1974; Oakey, 1977; Oakey and Elliott, 1982). The shear probes (as they will be called here) which were used in the present experiment are similar in design to those described by Osborn and Crawford (1980) but were built at the Bedford Institute of Oceanography. A piezobimorph beam senses lift fluctuations from velocity $u(t)$ perpendicular to the axis, as the probe moves axially through the water at a mean speed V. Two probes are used to measure two components of velocity shear. The output from each shear probe as a function of time is given by

$$E_0(t) = S_v \rho V u(t), \tag{2.1}$$

where S_v is a calibration factor, ρ is the density

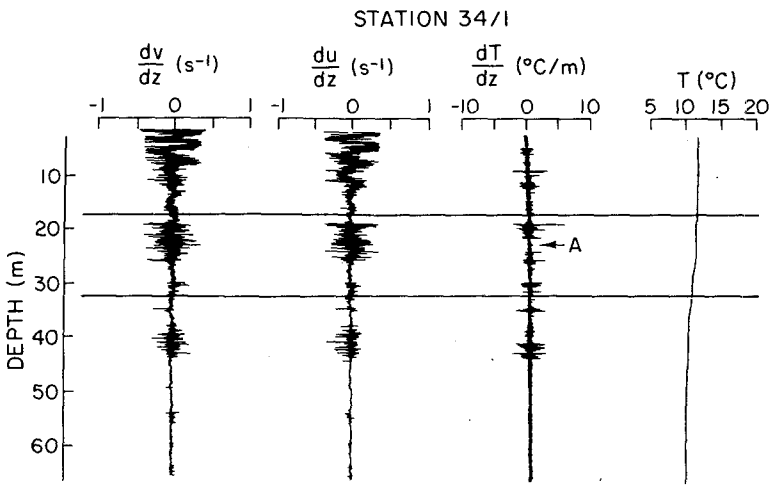

FIG. 1. A vertical profile (Station 34/1) showing velocity shear, temperature gradient and temperature. For the section, delineated by two horizontal bars, between 17 and 32 m, $\epsilon = 7 \times 10^{-8}$ m^2 s^{-3}, $\chi_\theta = 1.9 \times 10^{-7}$ °C^2 s^{-1} and $dT/dz = 5.7 \times 10^{-2}$ °C m^{-1}.

of water, and V is the mean vertical drop speed. The sensor is calibrated by measuring the output response obtained by oscillating the probe sinusoidally through a known angle in a laminar water jet of mean speed V.

The signals for both temperature and velocity shear are recorded in the derivative form as well as the direct form. Making use of the nearly constant vertical drop speed V and using Taylor's hypothesis give the temperature gradient as

$$\frac{dT}{dz} = \frac{1}{V}\frac{dT(t)}{dt}. \tag{2.2}$$

Similarly, for velocity shear one obtains

$$\frac{du}{dz} = \frac{1}{V}\frac{du(t)}{dt} = \frac{1}{V^2\rho S_v}\frac{dE_0(t)}{dt}. \tag{2.3}$$

A thorough description of the calibration errors and noise is deferred to the section on error analysis.

3. Selection of data for analysis

During the Joint Air Sea Interaction experiment (JASIN) in August–September 1978, in the Rockall Trough area northwest of Scotland ~250 vertical profiles of microstructure were obtained to depths of 50–100 m under a variety of wind-wave conditions and temperature-salinity structures. From these profiles ~600 10–15 m segments were analyzed to obtain estimates of turbulent energy dissipation. The data for the present discussion are a subset of ~25 of these segments chosen according to the following criteria. The basic considerations were that the spectra selected must be those with the best signal-to-noise ratio for the velocity spectrum while still resolving "all" of the temperature spectral variance. The analysis cut-off frequency was 100 Hz set by filters and discriminators within OCTUPROBE. The instrument drop speed was 0.6–0.8 m s^{-1} during much of the experiment, which meant that although the shear spectrum was resolved, the temperature-gradient spectrum, particularly at higher dissipation levels, was often cut off at high wavenumbers. Three representative time-series segments are shown in Figs. 1–3. These three stations indicate the variability of both $(\partial u'/\partial z)$ and $(\partial T'/\partial z)$ with depth. There is a lack of a one-to-one correspondence of velocity to temperature (e.g., A, Fig. 1). The 10–15 m depth interval was selected before the present study was anticipated and the source data were unavailable for what might have been a more appropriate choice. Sixteen blocks of data similar to those of Figs. 1–3 with dissipation ϵ ranging from 8×10^{-9}–10^{-7} m^2 s^{-3}, each resolving nearly all of the temperature gradient variance, were selected for the first part of the analysis to determine the universal constant q. For the second part of the analysis, where dissipation was estimated by fitting a Batchelor curve to the temperature-gradient spectrum, five others were included which had dissipation levels up to 5×10^{-7} m^2 s^{-3} but which resolved only ~75–80% of the temperature gradient variance. This was done in an attempt to extend the range of comparison of the two methods of determining ϵ.

4. Spectral computation

The first step in the data analysis was to compute power spectra for each component of velocity shear and temperature-gradient microstructure. This was accomplished by replaying the FM-multiplexed data

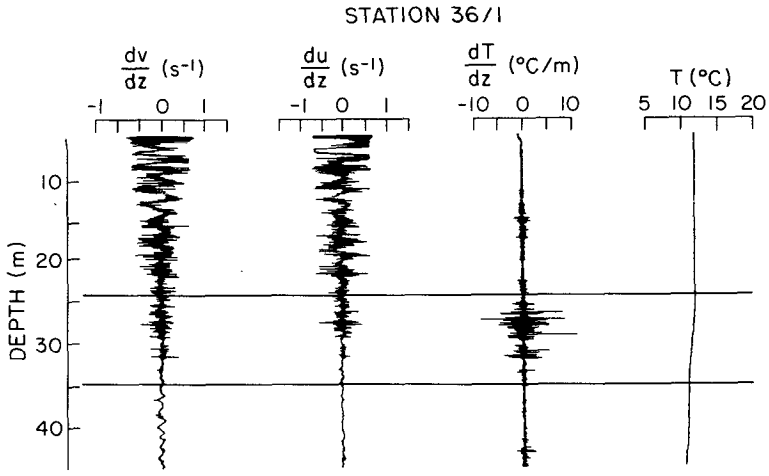

FIG. 2. A vertical profile for Station 36/1 similar to Fig. 1. In this case $\epsilon = 4.2 \times 10^{-8}$ m^2 s^{-3}, $\chi_\theta = 1.33 \times 10^{-6}$ °C^2 s^{-1} and $dT/dz = 8.4 \times 10^{-2}$ °C m^{-1}.

tape through a bank of filters and discriminators to reproduce the analog record. This analog time series was digitized at 200 Hz (Nyquist frequency of 100 Hz). This digital time series was converted to physical units by applying appropriate calibrations and scaling factors. Spectra were computed using blocks of 1024 points corresponding to a depth interval of ~3 m for a vehicle drop speed of 0.5–0.6 m s^{-1}. Several (usually five) blocks were averaged to provide the power spectrum for a depth interval of 10–15 m. Frequency response corrections were applied at the spectral stage to correct for the assumed ideal response of the differentiator circuits in OCTUPROBE, the response of filters and discriminators, and the frequency response of the sensors. The resultant power spectra [(physical units)^2 Hz^{-1} versus frequency (Hz)] were calculated in the one-third octave band-averaged form.

Fig. 4 illustrates a representative spectrum for velocity shear. The ordinate and abscissa have been converted to power (s^{-2} cpm^{-1}) and wavenumber (cpm) using the mean instrument drop speed V [e.g., $\hat{k} = f/V$ and $\phi(\hat{k}) = \phi(f)V$]. The correction for electronic response increases with frequency, being ~10(±6%) at 100 cpm. The shear-probe-response correction is applied assuming that the sensor has a response function equivalent to a single-pole filter with a cutoff scale λ_c. The correction is thus a mul-

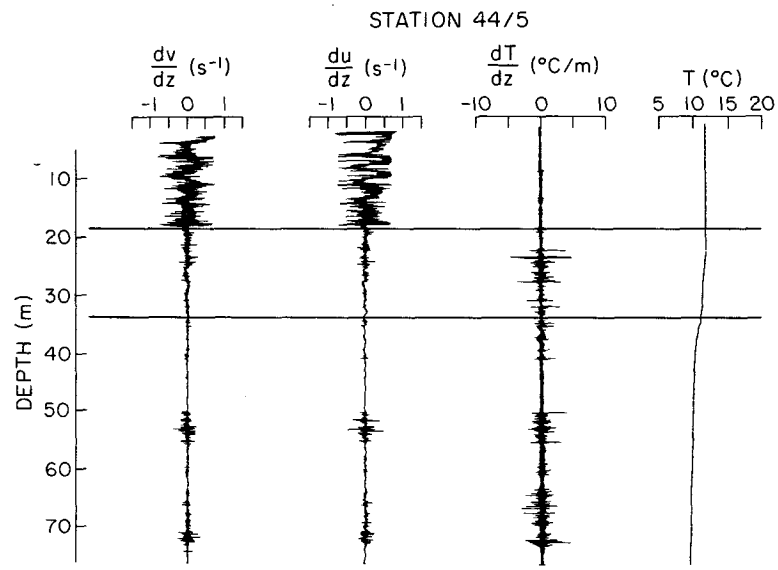

FIG. 3. A vertical profile for Station 44/5 similar to Fig. 1. In this case $\epsilon = 1.37 \times 10^{-8}$ m^2 s^{-3}, $\chi_\theta = 2.5 \times 10^{-7}$ °C^2 s^{-1} and $dT/dz = 3.98 \times 10^{-2}$ °C m^{-1}.

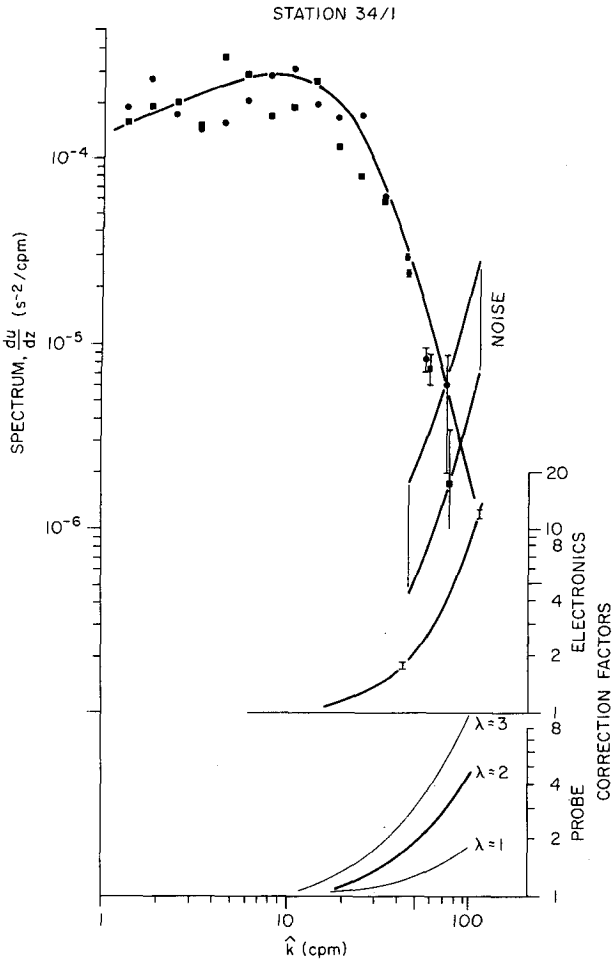

FIG. 4. The power spectrum of velocity shear for Station 34/1. The spectrum for shear sensor number one is shown as a solid circle, and for the perpendicular component measured by shear sensor number two as a solid square. The error bars reflect the corrections for noise (indicated as a band between the upper and lower noise estimate) and for electronic response. The magnitude and errors associated with the electronic response correction are shown below. The probe correction used (λ = 2 cm) is shown as the bold curve in the bottom figure. The corresponding corrections for λ = 1 cm and λ = 3 cm are indicated for comparison. The solid curve through the spectral estimates is Nasmyth's universal curve for $\epsilon = 7 \times 10^{-8}$ m^2 s^{-3}.

tiplier $[1 + (\hat{k}\lambda_c)^2]$. The value of λ_c is poorly known but our best estimate is λ_c = 0.02 m which is the value we have used. More detail leading to this choice is deferred to Section 7. The final correction applied to the spectrum is to subtract the noise. The noise curve was estimated from those sections of data where the signal was the lowest. The noise curve obtained from many very-low-noise blocks is consistent with the curve shown within a factor of 2 and is shown as two limiting curves, twice the curve used and one-half the curve used. The resultant spectral estimates for two components of shear (SH1 = solid circle, SH2 = solid square) are shown in Fig. 4 where the error bars include only the uncertainty in noise subtraction and electronic correction. Dissipation is obtained by integrating the corrected spectrum, and ϵ is calculated using this variance and the expression given in Eq. (1.3). The solid curve is the "universal" turbulence curve of Eq. (1.2) based on Nasmyth's data of Table A1 and ϵ from Eq. (1.3).

Fig. 5 illustrates a spectrum of temperature gradient corrected in a fashion similar to that previously described for velocity shear. The corrections for differentiator and filter-discriminator have been displayed as "electronic" spectral corrections and have an error of ±6% at 100 cpm. The thin-film-probe frequency response is determined by finding its response to a heated plume at several speeds (Fabula, 1968). The measured quantity in the calibration is

$$C_i = V_i^{0.64}\left(\frac{\Delta^2}{D}\right)_i,$$

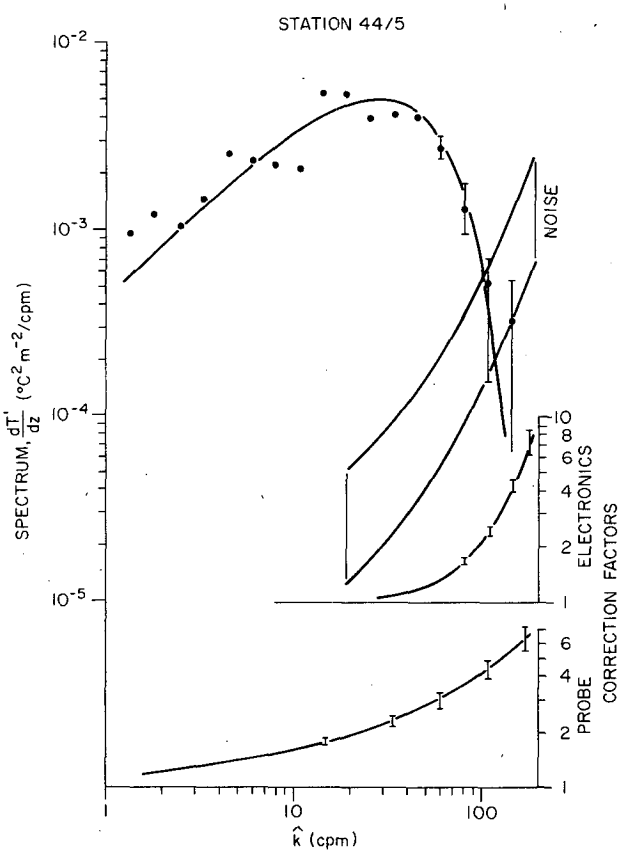

FIG. 5. The temperature gradient power spectrum for Station 44/5. The error bars include the indicated uncertainties in noise subtraction (indicated by the upper and lower estimates of the noise curve) and for electronic frequency response and probe correction. The correction for the transfer function of the electronic circuits is shown and, as well, the probe correction which was based on the calibration method of Fabula. The solid curve through the data is the Batchelor curve for ϵ measured using simultaneous velocity shear measurement and χ_θ from the integral of the temperature gradient spectrum.

where V is the speed at which the probe is driven through the plume, Δ is related to the boundary layer thickness, and D is the thermal diffusivity; $(\Delta^2/D)_i$, which has the dimensions of time, is measured using Fabula's theory at many (i) speeds and the quantity

$$C = n^{-1} \sum_{1}^{n} C_i$$

is found to be constant within ±15% for speeds from 0.20 to 1.5 m s^{-1}. The value of

$$\tau = \Delta^2 D^{-1} = C/V^{0.64},$$

where V is now the mean drop speed of OCTUPROBE for the section of data analyzed is used as the thin-film-probe correction parameter in the formula

$$A(\hat{k}) = A_{\text{MEAS}}(\hat{k}) \exp(\pi \hat{k} V \tau)^{1/2}. \qquad (4.1)$$

The ±15% error in τ translates to a ±5% error at 1 cpm and ±25% at 100 cpm. A noise curve was obtained from the quietest blocks of data measured, and the indicated noise region represents the uncertainty in this curve (from twice to one-half the curve used in the analysis).

The solid dots in Fig. 5 are the corrected spectral estimates with the error bars including the electronic correction, probe correction and noise subtraction.

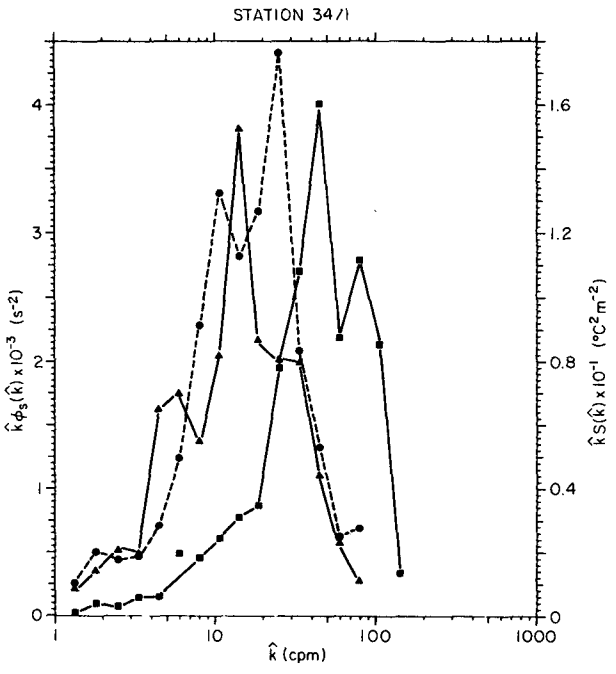

FIG. 6. The variance conserving spectral plot for Station 34/1. Two components of velocity shear are shown as shear one (solid dot) with $\epsilon_1 = 7.7 \times 10^{-8}$ m^2 s^{-3}, shear two (solid triangle) with $\epsilon_2 = 6.2 \times 10^{-8}$ m^2 s^{-3} and temperature gradient (solid square) with $\chi_\theta = 1.91 \times 10^{-7}$ °C^2 s^{-1}. The variance is the integral under these spectra and is used to determine ϵ and χ_θ.

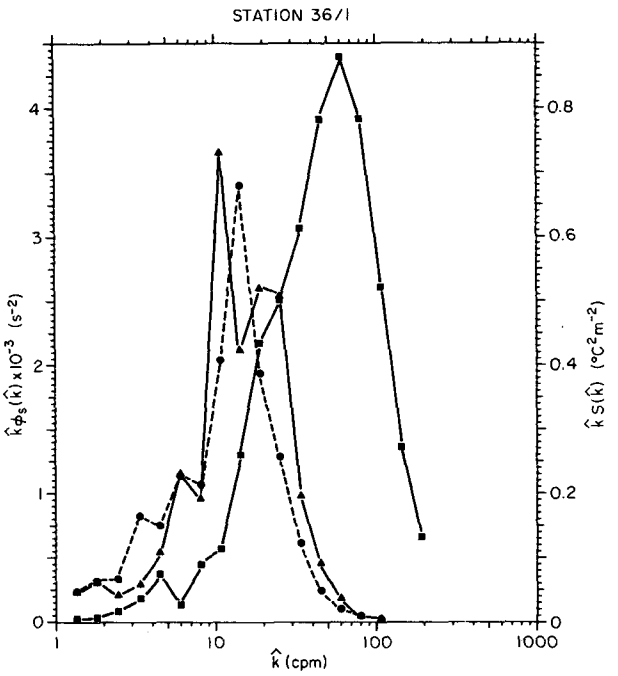

FIG. 7. The variance-conserving spectral plot for Station 36/1 similar to Fig. 6 with $\epsilon_1 = 3.9 \times 10^{-8}$ m^2 s^{-3}, $\epsilon_2 = 4.5 \times 10^{-8}$ m^2 s^{-3}, $\chi_\theta = 1.33 \times 10^{-6}$ °C^2 s^{-1}.

From this curve we obtain, by integration, the temperature-gradient variance and from this, calculate χ_θ using Eq. (1.6). The solid curve is the Batchelor spectrum computed using the value of ϵ from the simultaneous shear measurement to calculate k_B, the value of χ_θ from integrating the curve of Fig. 5. The value $q = 4.15$ was used in Fig. 5, which gave the best fit to the data above 10 cpm.

To illustrate the extent to which the spectra are resolved, three examples of data are shown in Figs. 6, 7 and 8, the variance-conserving plots of two components of velocity shear and temperature gradient for the three time series of Figs. 1, 2 and 3 respectively. In this presentation equal areas represent equal variance. There are differences in detail between du'/dz and dv'/dz, but the integral property ϵ agrees within ~ ±20%. In all cases the total variance is well resolved. Spectra such as these have been used in the analysis to estimate q.

5. Determination of q

Each of the 16 spectra selected to estimate the parameter q were normalized and plotted as $[S_{\text{MEAS}}(\hat{k}_l)/(\chi_\theta/k_B D)]$ versus the non-dimensional wavenumber k_l/k_B. The wavenumber $\hat{k}_l$ is a discrete value of $\hat{k}$; χ_θ was obtained from the integral of the temperature variance, and k_B was determined from Eq. (1.5) with ϵ determined from the average variance for the two measured spectra of velocity shear.

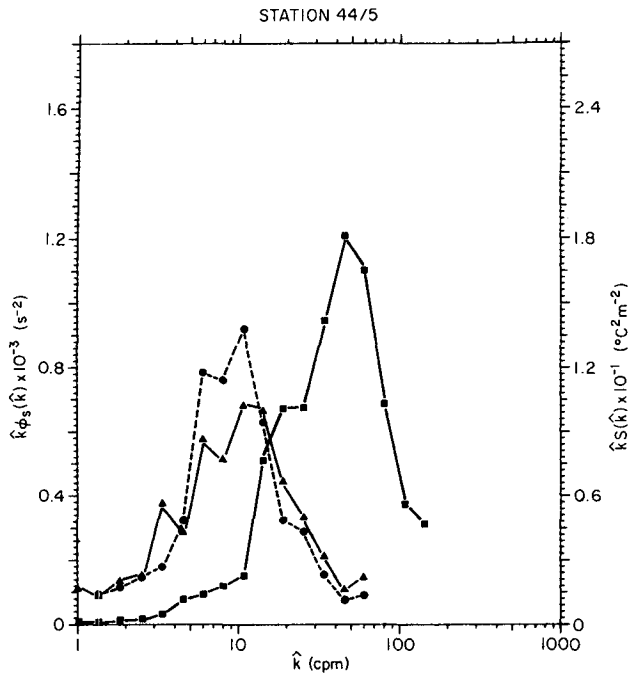

FIG. 8. The variance-conserving spectral plot for Station 44/5 similar to Fig. 6 with $\epsilon_1 = 1.4_1 \times 10^{-8}$ m^2 s^{-3}, $\epsilon_2 = 1.32 \times 10^{-8}$ m^2 s^{-3} and $\chi_\theta = 2.5 \times 10^{-7}$ °C^2 s^{-1}.

A scatter plot of these data is shown in Fig. 9a. A similar plot of the same data in variance-conserving form is shown in Fig. 10a. The best estimate of q was obtained by finding the least-square residual defined by

$$R(q) = \sum_{1}^{N} \sum_{l=1}^{j} \hat{k}_l^2 [S_{\text{MEAS}}(\hat{k}_l)/(\chi_\theta/k_B D) - (q/2)^{1/2} g(q, \hat{k}_l/k_B)]^2, \quad (5.1)$$

where $S_{\text{MEAS}}(\hat{k}_l)/(\chi_\theta/k_B D)$ is the normalized measured spectral intensity at a wavenumber $\hat{k}_l$, $(q/2)^{1/2} g(q, \hat{k}_l/k_B)$ is the value computed from Eq. (1.4), and N is the number of spectra. $R(q)$ was determined for values of $1 < q < 10$ in intervals of $\delta q = 0.05$. The values of l were chosen to include data for values of $\hat{k}$ between 10 and 150 cpm (excluding the last temperature-gradient spectral estimate which often has a large error bar because of the noise subtraction). This corresponds to $0.01 < \hat{k}/k_B < 0.15$. A plot of $R(q)$ vs q is shown in Fig. 11. It shows a minimum at $q = 3.7$. To illustrate the quality of the fit, the points of the scatter plot in Fig. 10a have been grouped in one-third octave bands and the mean and standard deviation determined. These are plotted for the variance-conserving form in Fig. 10b. Superimposed on these data in Fig. 10b are the Batchelor curves for $q = 1, 2, 3.7, 8$ with the curve for $q = 3.7$ the best fit, indicated as a bold solid line. A similar grouping for the points in Fig. 9a is shown in 9b along with the Batchelor curve for $q = 3.7$. Discrepancies between the curve and the data are evident and will be discussed later.

An alternate determination of the mean q was achieved by finding the best value for each spectrum by applying Eq. (5.1) to each spectrum individually [e.g., $N = 1$ in Eq. (5.1)]. The results of this computation are shown in Table 1. There is a wide vari-

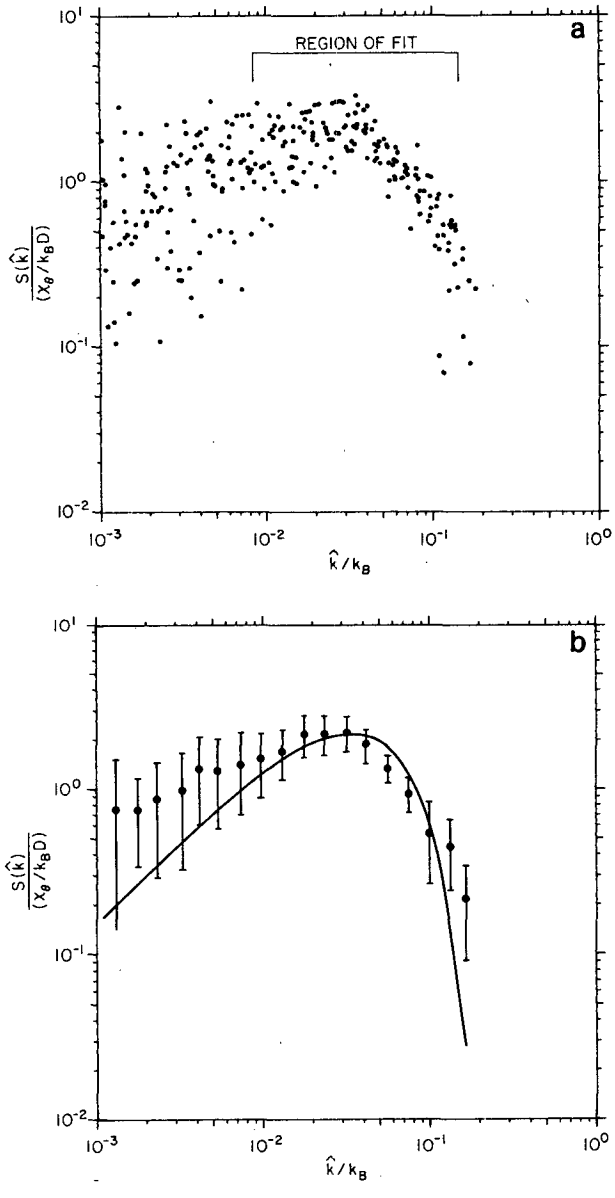

FIG. 9. (a) The scatter plot for temperature gradient data normalized to $(\chi_\theta/k_B D)$ versus the non-dimensional wavenumber $(\hat{k}/k_B)$. The plot includes for 16 spectra. The region over which a fit to the universal Batchelor form is indicated. (b) As in (a) except grouped into one-third octave bands with the mean in a band shown as a solid dot and where the error bars are the standard deviation within the band. The solid curve is the Batchelor curve which best fits the data for $q = 3.7$.

ation in the value of q which best fits individual spectra, from $q = 1.55$ for station 42/3(21–36 m) to $q = 6.95$ for station 34/1(17–32 m). The mean $q = 3.67$ is, not surprisingly, the same as the value obtained above for the ensemble and the standard deviation is 1.52.

6. Determination of ϵ from temperature gradient

An alternative but equivalent approach to the data is to assume that the value of q is a constant, and

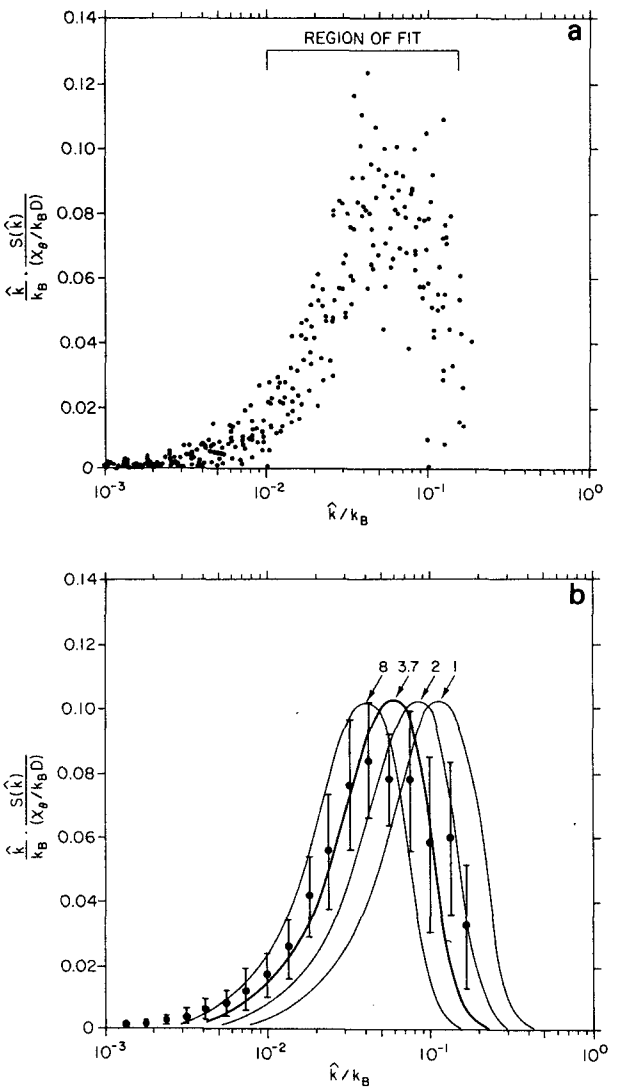

FIG. 10. (a) The scatter plot of the data of Fig. 9 is shown in variance-conserving form. The region over which the data was fit to the Batchelor form is indicated. (b) As in (a) except grouped in one-third octave bands with the band mean shown as a solid dot and the error bars are the standard deviation within the band. The curves for $(q/2)^{1/2}\hat{k}/k_B g(q, \hat{k}/k_B)$ are shown for different values q spanning the "best fit" curve for $q = 3.7$ shown more boldly.

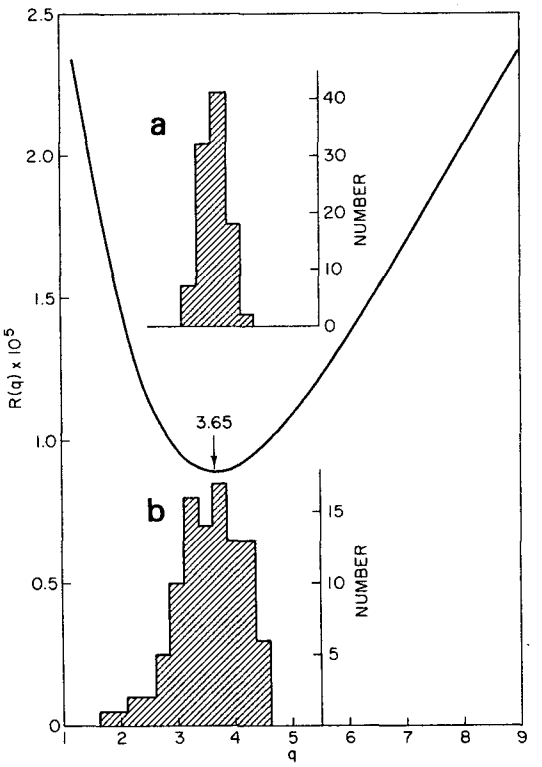

FIG. 11. The plot of the least-squares residual curve $R(q)$ shown as a solid curve plotted versus q. The minimum at $q = 3.7$ represents the "best fit." (a) The sensitivity of the calculation of $R(q)_{MIN}$ to the estimated maximum random errors: $\delta V = 0.05$, $\delta\epsilon = 0.30$, $\delta\chi_\theta = 0.20$ obtained from a Monte Carlo calculation which gives $q = 3.65 \pm 0.20$. (b) A similar test of the sensitivity of $R(q)_{MIN}$ to systematic errors: $\delta\epsilon = 0.32$, $\delta X = 0.17$ which gives $q = 3.6 \pm 0.59$.

is known, and to find the Batchelor spectrum which best fits each measured spectrum. From this best fit we obtain a cutoff scale k_B from which we can estimate ϵ since

$$\epsilon = k_B^4 \nu D^2. \tag{6.1}$$

As before, $\nu = 1.27 \times 10^{-6}$ m^2 s^{-1} is the kinematic viscosity and $D = 1.39 \times 10^{-6}$ m^2 s^{-1} is the thermal

TABLE 1. Determination of q for individual spectra.

Station	q	Station	q
18/5 (46–66)*	1.70	38/1 (19–34)	4.55
32/1 (67–84)	5.65	38/4 (27–45)	2.15
34/1 (17–32)	6.95	42/3 (21–36)	2.35
34/2 (17–31)	3.00	42/3 (36–51)	1.55
36/1 (25–35)	4.70	44/2 (20–30)	5.00
36/2 (25–35)	2.80	44/5 (18–33)	4.15
36/3 (25–37)	3.90	48/3 (16–23)	4.15
36/4 (24–34)	4.00	48/9 (24–30)	2.15
Mean q	3.67 ± 1.52		

* Depth interval (m) shown in parentheses.

TABLE 2. Summary of experimental data.

Station	Depth (m)	$d\bar{T}/dz$ (°C m^{-1})	χ_θ (°C^2 s^{-1})	Cox Number	ϵ_{SH} (m^2 s^{-3})	ϵ_B (m^2 s^{-3})	ϵ_B/ϵ_{SH}	Γ
18/5	46-66	10.6	28.6	30	6.8	23.6	3.47	0.259
24/3	44-55	4.17	13.6	94	10.0	8.3	0.83	0.213
24/5	8-12	3.11	73.4	910	80.4	31.0*	0.39	0.192
28/4	38-55	8.1	79.7	146	20.0	70.5	3.53	0.321
30/1	5-21	0.487	140.	71000	315.	433.0*	1.37	0.596
32/1	67-84	1.97	22.1	685	27.4	16.8	0.61	0.267
34/1	17-32	5.7	19.1	69	69.8	27.2	0.39	0.031
34/2	17-31	5.7	70.5	256	80.8	121.	1.49	0.100
34/4	18-33	4.7	108.	586	133.	158.	1.19	0.113
34/5	18-33	5.7	40.1	146	130.	77.1	0.59	0.035
36/1	25-35	8.4	133.	224	42.1	38.1	0.91	0.246
36/2	25-35	15.9	183.	86	31.5	68.0	2.16	0.239
36/3	25-37	7.6	134.	281	75.2	96.5	1.29	0.153
36/4	24-34	8.9	142.	216	153.	170.	1.11	0.068
38/1	19-34	11.2	572.	548	69.5	68.6	0.99	0.480
38/3	11-27	2.55	144.	2662	362.	161.0*	0.45	0.102
38/4	27-45	13.2	168.	115	27.4	77.2	2.82	0.303
42/3	21-36	6.45	73.9	213	32.5	52.5	1.62	0.230
42/3	36-51	2.06	104	2930	31.8	38.9	1.22	1.037
42/4	4-21	0.463	36.4	20300	392.	320.0*	0.82	0.131
42/5	4-20	0.243	29.3	59300	516.	333.0*	0.65	0.153
44/2	20-30	8.5	70.2	116	49.5	28.8	0.58	0.109
44/5	18-33	3.98	25.0	190	13.7	11.6	0.85	0.300
48/3	16-23	1.3	22.9	1720	30.6	20.4	0.67	0.376
48/9	24-30	9.0	178.	260	30.8	43.3	1.41	0.420
		$\times 10^{-2}$	$\times 10^{-8}$		$\times 10^{-9}$	$\times 10^{-9}$		
						Mean	1.26	0.259
							±0.88	±0.214

* Temperature variance not fully resolved.

conductivity. This calculation has been done using a value of $q = 4$ for each of the data sets listed in Table 2. The value of $q = 4$ was chosen for convenience. It could be any reasonable value, but is consistent with the value determined here and the value 3.9 ± 1.5 reported by Grant *et al.* (1968). An error in the choice of q represents a systematic error in the derived values of ϵ from Eq. (6.1) since $\epsilon \propto q^2$.

The graphical method of fitting "universal" curves is described by Stewart and Grant (1962). The reference curve, in this case the Batchelor curve, $(q/2)^{1/2} g(q, \hat{k}/k_B)$, for $q = 4$ is plotted on log-log paper, versus the nondimensional wavenumber $\hat{k}/k_B$ and a convenient reference point marked. The data $[S_{MEAS}(\hat{k})$ vs $\hat{k}]$ are plotted on log-log paper of the same size. A line of slope −1 through the point

$$\left[(\nu D^2)^{-1/4}, \frac{\chi_\theta}{D}(\nu D^2)^{1/4}\right]$$

is drawn on the experimental curve. This is illustrated in Fig. 12 for station 36/1. The "universal" curve is aligned to give the best fit to the experimental data with the constraint that the reference mark (+) on the universal curve must be on the line of slope −1. This method provides a ratio of the axes of the universal curve and the data since both are plotted in log-log form. The reference $\hat{k}/k_B$ which corresponds to a wavenumber $\hat{k}$ for the data is obtained and from this, by ratio, the experimental value of k_B is determined. Dissipation ϵ_B is calculated from Eq. (6.1) where the subscript B denotes that it is determined from the Batchelor spectral fit to temperature-gradient data. For the sample shown in Fig. 12 the reference point is $\hat{k}/k_B = 0.1$ and the value of $\hat{k}$ = 112 cpm. From this, k_B = 1120 m^{-1} and $\epsilon_B = (1120)^4 \times (1.27 \times 10^{-6}) \times (1.39 \times 10^{-7}) = 3.8 \times 10^{-8}$ m^2 s^{-3}. The corresponding value obtained from the shear-probe measurements was $\epsilon_{SH} = 4.2 \times 10^{-8}$ m^2 s^{-3}. Only a few examples agree this well!

The previous graphical analysis was done for 20 examples where the temperature variance was well resolved. These data are listed in Table 2 which also includes the essential specifications of each profile analyzed including depth interval, mean gradient, χ_θ and, in particular, the values of ϵ_{SH} and ϵ_B. The agreement between the two methods is illustrated in Fig. 13 which shows the 20 values of ϵ_B plotted as solid circles against the corresponding values of ϵ_{SH}. The solid line represents "perfect" agreement. Five other spectra were used for which only 70–80% of the temperature-gradient variance was resolved. These were analyzed with the previously described graphical method with the relaxed constraint that

the reference mark could be moved above the line of slope −1 (by up to 20%). These estimates of ϵ_B, which are higher than the previous 20 (and thereby explain the cutoff of the temperature spectrum), are plotted as solid squares on Fig. 13.

7. Error analysis

This section will attempt to describe as quantitatively as possible the sources of error associated with the determined spectral shapes, the magnitude of the errors in integral quantities such as ϵ and χ_θ, and an estimate of the confidence limits associated with the determination of q. The errors have been categorized into "random" errors associated with measurement uncertainties from data block to data block and "systematic" errors which are non-random in the sense that the errors apply equally to all sets of data. These errors are summarized in Table 3, and the discussion to follow will describe the methods used to estimate these errors.

a. Mean drop speed

The mean drop speed V is determined from the change in the measured pressure signal over the time interval of the analysis block of data. Uncertainties in the measured voltage, time interval and sensor calibration contribute 1–2%. The difference in actual speed $V(z)$ at any point in the block of data may vary from the mean by as much as ±2% as a result of non-constant drop speed. A further uncertainty in the water speed relative to the probe as a result of wave motion or blockage is difficult to estimate. Combining these sources, the best estimate of the error in V is ±5%.

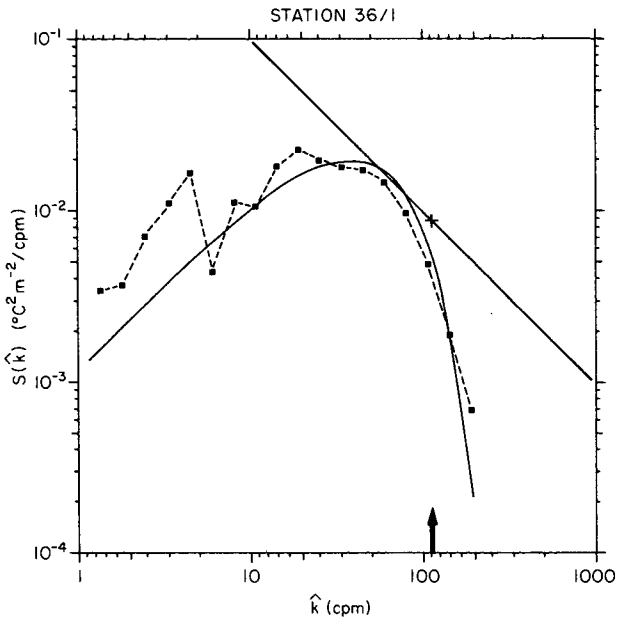

FIG. 12. Illustrates the method of obtaining a cutoff scale $\hat{k}$ for temperature gradient. The reference mark (+) at $\hat{k}/k_B = 0.1$ of the universal curve indicated in Fig. 9b is constrained to the line of slope −1 in obtaining the best fit to the data. In this case, the best fit is at 112 cpm indicated by an arrow. This graphical technique of fitting the Batchelor curve to an experimental data set allows one to estimate k_B (in this case 1120 m^{-1}) and hence the dissipation ϵ.

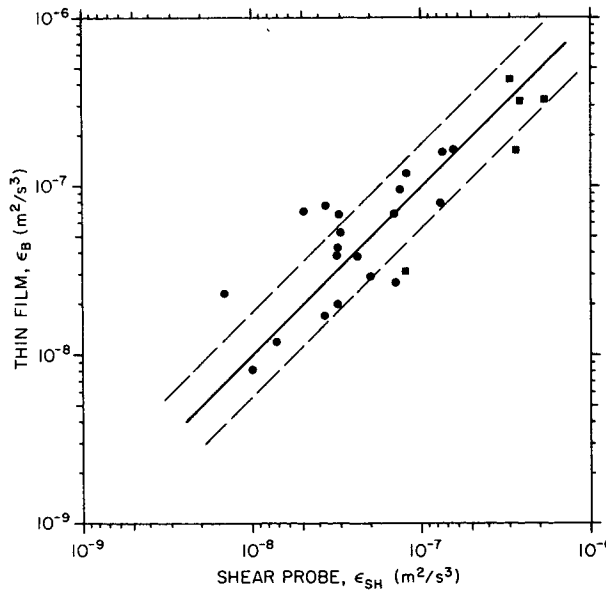

FIG. 13. Dissipation obtained from temperature gradient measurements plotted versus the simultaneously obtained quantity from shear probe measurements. The solid line represents perfect agreement, the two dashed lines the factor 1.8, and $(1.8)^{-1}$ represent the estimated measurement uncertainties in ϵ_B and ϵ_{SH} (exclusive of questions of isotropy).

b. Velocity shear and dissipation

An error in the mean speed V will cause an error four times as large in the calculated dissipation, as is shown by Eq. (2.3) since the power spectrum is $\overline{(du'/dz)^2}$. This error occurs randomly in our measurements and contributes ±20%. Shear probes are calibrated by sinusoidally changing their angle of attack to a mean flow of speed V which is generated by a laminar free jet. The repeatability between calibrations is always better than ±5% and the rms scatter for several calibrations of many probes is ±2.5%. The systematic errors associated with probe calibration are difficult to estimate but, to acknowledge them, the above error has been (optimistically) doubled, yielding a calibration error of ±5% in amplitude or ±10% in power. The uncertainty in the gain of electronic amplifiers, filters and other components of the data-recording playback system of ±2% can contribute another ±4% error to the measured ϵ. The transfer function for filters and differentiator circuits is shown in Fig. 4. The correction factor at 100 cpm

TABLE 3. Error summary.

Variable	Error source	Random	Systematic	Qualifiers
V	Mean drop speed	±5%		
ϵ	V	±20%		
	Probe calibration		±10%	
	Electronic calibration		±4%	
	Electronic frequency response		±3%	
	Probe frequency response		±15%	±10% at $\epsilon = 10^{-8}$ m^2 s^{-3} ±20% at $\epsilon = 10^{-7}$ m^2 s^{-3}
	Noise subtraction	±7%		
	max error	±27%	±32%	
	rms error	±21%	±19%	
χ_θ	V	±10%		
	Probe calibration		±1.6%	
	Electronic calibration		±4%	
	Electronic and probe frequency response		±11%	
	Noise subtraction	±10%		
	max error	±20%	±17%	
	rms error	±15%	±12%	

may be as large as 10 in power with an uncertainty of ±6% and progressively smaller at lower wavenumbers where, for example, at 15 cpm the correction is ~1.2 and the error ±2%. The spectral shape is affected at these levels by this error source. In the integral sense where the majority of the variance occurs at wavenumbers <50 cpm the contribution to the error in the determination of the variance is ±3%. The spatial response of the sensor is very poorly known. From geometrical considerations (Osborn and Crawford, 1980), with the sensitive length-of-probe-tip of 1 cm, a cutoff equivalent to $\lambda_c = 2$ cm is not unreasonable. A preliminary study at the Bedford Institute indicated that $\lambda_c = 2 \pm 1$ cm by comparing the shear probe to a thin-film ×-probe. A comparison of the spectral shape using a correction of $\lambda_c = 2$ cm agrees reasonably with the universal curve of Nasmyth (Oakey and Elliott, 1982). The lack of a definitive experiment to define λ_c precisely has led to the caveat that because of the probe's size it cannot have a value of $\lambda_c < 1$ cm and a variety of circumstantial evidence indicates it to be <3 cm. The choice of $\lambda_c = 2$ cm is the compromise chosen. Spectral shapes will be affected more at high wavenumbers than at low and with the assumption of a simple single-pole form will have a range of corrections shown in Fig. 4. Because this is a log-log plot, an error in the value of λ_c from the assumed value of 2 will add to or subtract from the curve presented within the limits of the error band shown below. In the determination of ϵ, the error resulting from λ_c at each wavenumber is weighted by the variance at that wavenumber. Since the peak of the dissipation curve is at a higher wavenumber for higher dissipation levels, the integrated error is larger at higher values of ϵ. Using the probe correction curve of Fig. 4 and the "universal" turbulence spectrum of Table A1 one finds the error in ϵ (from λ_c) to be 4% for $\epsilon = 10^{-9}$ m^2 s^{-3}, 10% for $\epsilon = 10^{-8}$ m^2 s^{-3}, 20% at $\epsilon = 10^{-7}$ m^2 s^{-3} and 36% at $\epsilon = 10^{-6}$ m^2 s^{-3}. Since the data for this experiment are mostly between 10^{-8} and 10^{-7} m^2 s^{-3}, the number quoted in the table is ±15%. The final source of error is that due to the uncertainty of the noise curve estimated from many blocks of data with the lowest measured signals. The curve selected had points scattered above and below it by a factor of 2 which was accepted as the estimate of this noise curve shown in Fig. 4. The error bars on the data points reflect this noise uncertainty. The scatter in estimates of variance using this noise curve produced a value of ±7% for the data presented in this paper.

In summarizing the combined effects of these errors, random errors may contribute a maximum error of ±27% (and an rms error of 21%). The systematic errors contribute a maximum of ±32% (or an rms of ±19%). The combination may yield a maximum of ±59% (or an rms of ±30%). There is the further consideration of the accuracy of the determination of ϵ from Eq. (1.3) and assumptions of isotropy which alone may introduce an error of ±50% into our values of ϵ. The conclusion is (optimistically) that ϵ is measured to within a factor of 2.

c. *Temperature gradient and* χ_θ

For temperature-gradient measurements the uncertainty in the mean drop speed V causes a random error twice as large in the calculation of variance or, alternately, χ_θ, as indicated by Eq. (1.6). The probe calibration is accurate to ±0.2°C for 25°C full scale which provides a systematic error in the determi-

nation of χ_θ since the same probe and electronics were used throughout this experiment. The calibration of electronic bridges, filters and discriminators can lead to a further ±4% uncertainty in the variance. The spectral data are corrected for the electronic transfer function as indicated in Fig. 5. The error in this correction increases with wavenumber (or frequency) to ±6% at 100 cpm. To correct the spectral intensities for the response of the thin-film probe the measured spectral intensities are multiplied by a factor

$$C = \exp[(\pi \hat{k} V \tau)^{1/2}], \tag{7.1}$$

as defined in (4.1). The equivalent time constant τ determined by Fabula's method (Fabula, 1968) as defined earlier has an uncertainty of ±15%. From (7.1), for a fractional error τ of $\delta\tau/\tau$ there is a corresponding fractional error in C given by

$$\frac{dC}{C} = \frac{(\pi \hat{k} V \tau)^{1/2}}{2} \frac{\delta\tau}{\tau}.$$

Thus, at 1 cpm the error in the correction is 1.4%, while at 100 cpm it is 15%. This is shown in Fig. 5. Using these error estimates for electronic and probe corrections and computing the variance-weighted error in the value of χ_θ for many of the spectra lead to an estimate of ±11% in the value of χ_θ from this source. The noise "curve" shown in Fig. 5 was obtained by examining the lowest-temperature-gradient blocks available. The upper limit is twice the curve used, and the lower limit is one-half the curve used. Data points for low-noise blocks analyzed were between these limits. The error bars on the plotted points of Fig. 5 reflect the uncertainty from noise, probe and electronic frequency response. The variance under the noise curve integrated to 100 cpm was equivalent to a $\chi_{NOISE} \simeq 2 \times 10^{-8}$ °C^2 s^{-1}. The associated factor-of-2 uncertainty in this quantity leads to an rms error of ±10% in χ_θ resulting from errors in noise subtraction for the 16 sets of data in Table 2.

In summary, random analysis errors lead to an estimate of ±20%, systematic sources to ±17% for a maximum error of ±37% in the values of χ_θ. There is, of course, the question of applicability of Eq. (1.6) for turbulence which is not isotropic, and an unspecified but possibly large error depending on the deviation from isotropy.

d. *The determination of q*

The determination of q by Eq. (5.1) has been discussed previously. The results of $R(q)$ vs q for the whole data set shown in Fig. 11 indicate that (in the least-square sense) $q = 3.7$. The results of a similar analysis for individual spectra using Eq. (5.1) are listed in Table 2. From this table $q = 3.67 \pm 1.52$. If q is a constant and the error in its determination is a result of random and systematic errors in V, ϵ and χ_θ, it is instructive to assess the effect of these errors. This has been done by finding the sensitivity of the minimum in $R(q)$ to both random and systematic errors using a simple Monte Carlo technique. For the maximum random errors, $\delta V = \pm 5\%$, $\delta\epsilon = \pm 30\%$, $\delta\chi_\theta = \pm 20\%$, the computation was made by ascribing a random Gaussian-distributed error to each V, ϵ and χ_θ of the 16 sets of data used in the computation. This was done 100 times to yield the histogram of q values shown in Fig. 11A. The histogram with mean $\bar{q} = 3.65$ indicates that random errors yield a standard deviation $\sigma = 0.20$.

A similar computation was made for the systematic errors in ϵ and χ_θ. However, in this case the same random Gaussian-distributed error was applied uniformly to each ϵ and χ_θ for the 16 spectra used in the calculation. For 100 determinations using the maximum systematic error $\delta\epsilon = 32\%$ and $\delta\chi_\theta = 17\%$, the histogram in Fig. 11B indicates a mean $\bar{q} = 3.6$ and a contribution to the standard deviation $\sigma = 0.59$. The determination of q is less dependent on the random error sources than on the systematic errors.

The sum of errors in q which may arise from random and systematic sources according to this Monte Carlo sensitivity analysis indicate $q = 3.65 \pm 0.8$. This is much less than the observed scatter from Table 2 of $q = 3.67 \pm 1.52$ and indicates a variability not ascribable to experimental errors.

e. *Graphical determination of* ϵ

The largest source of error is the determination of the best fit of the "universal" Batchelor curve to the data curve. The graphical method is subjective and may have an associated error of ±10%, which by Eq. (6.1) results in ±40% in ϵ_B. An error in χ_θ (if it is fully resolved) should cause little error in ϵ_B because it is essentially included, then divided out. An error in V of ±5% can yield an error in $\hat{k}$ of ±5% and therefore from Eq. (6.1) an error in ϵ_B of ±20%. However, an equal error occurs in ϵ_{SH} from Eq. (2.3) so that in the ratio of ϵ_B/ϵ_{SH} this error drops out. Accepting the error as ±40% in ϵ_B and using the sum of the rms random and systematic errors (21% + 19%) as the probable error in the measurement of ϵ_{SH} (±40%) yields the error in the ratio $R = \epsilon_B/\epsilon_{SH}$ of

$$\frac{\delta R}{R} = \left|\frac{\delta\epsilon_B}{\epsilon_B}\right| + \left|\frac{\delta\epsilon_{SH}}{\epsilon_{SH}}\right| = 0.80. \tag{7.2}$$

In Fig. 13 the solid line ($R = 1$) is bracketed by dashed parallel lines of $R = 1.8$ and $R = 1.8^{-1}$ representing the error limit of Eq. (7.2). The majority of the observed ratios fall within these limits. As shown in Table 3, the mean and standard deviation of the observed ϵ_B/ϵ_{SH} ratios is 1.26 ± 0.88.

8. Discussion and conclusions

Several questions can be addressed on the basis of the results presented. One can examine the extent to which q is a universal constant. Second, it is possible to discuss how well the shape of temperature-gradient spectra is described by the Batchelor spectrum. And finally, one can ask whether dissipation rates can be estimated from temperature-gradient microstructure alone.

The least principal rate of strain q of the Kolmogoroff velocity spectrum has been considered to be a universal constant. Batchelor's derivation (Batchelor, 1959) was done in terms of a three-dimensional spectrum and the present analysis assumes isotropy and uses the derived one-dimensional form. If there is considerable anisotropy, q may vary as a result. From a practical point of view, it may be difficult to distinguished experimental errors from anisotropy effects. The values of q which were obtained for each spectrum individually are listed in Table 2. These values indicate that $q = 3.67 \pm 1.52$. The estimated error in q resulting from the sensitivity of the technique to errors in V, ϵ and χ_θ was determined by a simple Monte Carlo method. This yielded the result that $q = 3.7 \pm 0.8$, based on the estimates of maximum error in Table 3. Thus the measured scatter in q is larger than that expected from combined random and systematic errors (i.e., 1.52 compared to 0.8). It must be emphasized that the error estimates do not include deviations from isotropy in the calculation of χ_θ and ϵ. One may then speculate that the difference between the standard deviation of measured values of q and the estimated experimental errors results from anisotropy. The difference is ± 1.28 [in the rms sense, i.e., $(1.5^2 - 0.8^2)^{1/2}$]. The effect of systematic errors in ϵ (32%) and χ_θ (17%) yielded an error in q of ± 0.59 (16%) as indicated in Fig. 11b. Thus an error due to anisotropy of the order of $\pm 75\%$ would be sufficient to explain the additional scatter of ± 1.28 (35%) observed in q.

The shapes of the individual temperature-microstructure spectra are consistent with the Batchelor spectral form when normalized using the independently measured dissipation to determine the cutoff wavenumber k_B. An example is shown in Fig. 5 for Station 44/5 where the fit is achieved with $q = 4.15$. The agreement is in a sense surprising because regions of large temperature gradients are not in one-to-one correspondence to regions of large velocity microstructure. This is evident in Fig. 1 at the level marked A. If a follow-on analysis were done it might benefit from selecting data in shorter records and examining the statistics on a scale more characteristic of the generation scales of microstructure.

The composite spectrum of Fig. 9b is compared to the Batchelor form for $q = 3.7$, the value which was the "best-fit" to the data from the sixteen spectra used in the calculation. The fit is not as good as for individual spectra as a result of both random and systematic errors in V, ϵ and χ_θ and, as discussed previously, the possible variations in q as a result of anisotropy. The errors in V and ϵ will result in improperly normalizing the spectra to the correct nondimensional wavenumber $\hat{k}/k_B$. This effectively broadens the peak in the variance-conserving spectra $\hat{k}\phi(\hat{k})$ of Fig. 10b (or flattens the spectrum in the $\phi(\hat{k})$ form of Fig. 9). This may explain part of the disagreement between the universal Batchelor form and the measured data. It is interesting to note, however, that Williams and Paulson (1977) observed a similar spectral form (their Fig. 11) in measurements in air. Using the standard deviation of the data points as a measure of σ the data are low near the peak of the Batchelor curve and high above. In the "roll-off" portion of the spectrum ($\hat{k}/k_B > 0.01$) the Batchelor curve is consistent with the data at ± 2 standard deviations.

In the $+1$ portion of the spectrum, the data are higher than the Batchelor curve. This is in agreement with previous work of Dillon and Caldwell (1980) who showed similar results for Cox numbers <500. In the present study the median Cox number is ~250. In this low wavenumber region effects such as stratification may be important in defining the spectral shape even though at high wavenumbers the spectral roll-off depends only on the local dissipation rate.

The final question posed in the opening paragraph of the discussion is whether dissipation levels can be estimated by temperature-gradient microstructure measurements alone. This technique has been explored extensively by Dillon and Caldwell (1980) and Caldwell *et al.* (1980). Caldwell *et al.* (1981) have shown that, consistent with their method, the Batchelor wavenumber determines the cutoff wavenumber in vertical temperature gradient spectra in a constant-stress bottom boundary layer. The results of the present experiment, summarized in Fig. 13, show that when dissipation ϵ_B is determined from well-resolved temperature-gradient spectra it agrees within a factor of 2 to the direct measurement of dissipation from velocity shear, ϵ_{SH}. It is tempting to apply these results to oceanic studies under a wide variety of regimes. While the results are applicable to active microstructure patches such as those chosen here, others which may be in a decaying state and more anisotropic may show less consistent agreement. More proof will be required before this generalization can be made.

Lilly *et al.* (1974) and Weinstock (1978) have used a scaling for vertical diffusivity which has the form

$$K_z = \Gamma\epsilon/N^2, \tag{8.1}$$

where N is the Brunt-Väisälä frequency. Lilly *et al.* (1974) found $\Gamma = 0.33$ from atmospheric measure-

ments. Weinstock (1980) proposed that $\Gamma = 0.8$ on theoretical grounds. It is this latter value which is used by Caldwell *et al.* (1980) in their calculation of dissipation from temperature-gradient measurements. On energy arguments Osborn (1980) proposed a vertical eddy coefficient for density of

$$K_\rho < 0.2\epsilon/N^2. \tag{8.2}$$

If the eddy coefficients for different scalar variables are the same (Munk, 1966) then there are three approaches with different values of Γ.

The factor Γ can be estimated from the data of Table 2 in the following way. The arguments of Osborn and Cox (1972) lead to the vertical eddy diffusivity

$$K_z = (2 \pm 1)D\frac{\overline{(\partial T'/\partial z)^2}}{(\partial \bar{T}/\partial z)^2}, \tag{8.3}$$

where D is the thermal diffusivity, $\overline{\partial T'/\partial z^2}$ the temperature gradient variance, $\partial \bar{T}/\partial z$ the mean temperature gradient, and the factor (2 ± 1) allows for departures from isotropy. Making the assumption that the Brunt-Väisälä frequency can be obtained from the temperature gradient, one can write

$$N^2 = \frac{g}{\rho}\frac{\partial \rho}{\partial z} = g\alpha\frac{\partial T}{\partial z}, \tag{8.4}$$

where $\alpha = 2 \times 10^{-4}\ ^\circ\mathrm{C}^{-1}$ is the coefficient of thermal expansion. Expressing the variance in Eq. (8.3) in terms of χ_θ one can write

$$\Gamma = \frac{N^2 K_z}{\epsilon} = g\alpha(\tfrac{1}{3} \pm \tfrac{1}{6})\frac{\chi_\theta}{\epsilon\dfrac{\partial \bar{T}}{\partial z}}. \tag{8.5}$$

An alternate derivation of this equation was provided the author by Greg Holloway (personal communication, 1981). These values Γ (ignoring the uncertainty $\pm \frac{1}{6}$) are calculated and listed in Table 2. The mean and standard deviation are 0.259 ± 0.21 (or 0.235 ± 0.14 ignoring the largest and smallest). This value is consistent with the values 0.20 and 0.33 used by Osborn (1980) and Lilly *et al.* (1974), respectively, but is not consistent with that proposed by Weinstock (1980). The scaling can be represented by the measurements of this experiment as

$$K_z = (1 \pm 0.5)(0.24)\epsilon/N^2. \tag{8.6}$$

The quantity Γ is a mixing coefficient representing the ratio of potential energy to kinetic energy dissipation. To show more clearly the distribution of Γ a histogram of the values in Table 2 is presented in Fig. 14. It would be most interesting to examine the variability of this quantity in a much larger range of oceanic regimes.

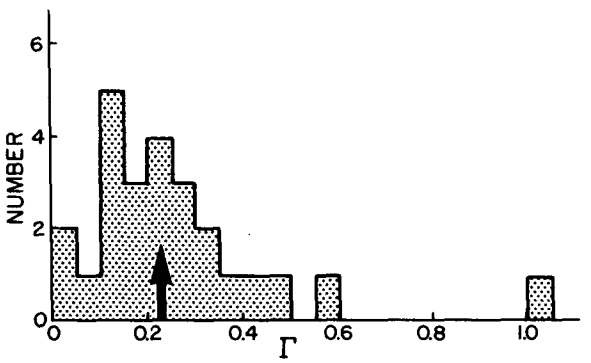

FIG. 14. Histogram of the number of occurrences of the mixing coefficient Γ. The mean is indicated by an arrow.

TABLE A1. Universal velocity spectra.

$\hat{k}/k_s$	$F(\hat{k}/k_s)$	$F_2(\hat{k}/k_2)$	$G_2(\hat{k}/k_s)$
2.83×10^{-4}	1.254×10^5	1.671×10^5	0.5285
5.03_3	4.799×10^4	6.397×10^4	0.6397
8.95_0	1.842×10^4	2.455×10^4	0.7763
$1.59_2 \times 10^{-3}$	7.050×10^3	9.404×10^3	0.9404
2.83_0	2.699×10^3	3.598×10^3	1.138
5.03_3	1.036×10^3	1.380×10^3	1.380
8.95_0	3.964×10^2	5.320×10^2	1.682
$1.59_2 \times 10^{-2}$	1.490×10^2	2.302×10^2	2.302
2.83_0	3.574×10^1	6.880×10^1	2.176
5.03_3	5.600×10^0	1.373×10^1	1.373
7.97_7	7.214×10^{-1}	2.101×10^0	0.5278
$1.26_4 \times 10^{-1}$	6.580×10^{-2}	2.127×10^{-1}	0.1342
1.59_2	1.812×10^{-2}	6.161×10^{-2}	0.0616
2.00_4	4.552×10^{-3}	1.570×10^{-2}	0.0249
2.52_2	1.197×10^{-3}	4.011×10^{-3}	0.0101

$k_s = (\epsilon\nu^{-3})^{1/4}$, $\hat{k} = f/V$

Velocity spectra

$\phi_{11}(\hat{k}) = (\epsilon\nu^5)^{1/4}F(\hat{k}/k_s)$ $[(\mathrm{m\ s^{-1}})^2\ (\mathrm{cpm})^{-1}]$

$\phi_{22}(\hat{k}) = (\epsilon\nu^5)^{1/4}F_2(\hat{k}/k_s)$ $[(\mathrm{m\ s^{-1}})^2\ (\mathrm{cpm})^{-1}]$

Shear or gradient spectrum

$(2\pi\hat{k})^2\phi_{22}(\hat{k}) = k_s^2(\epsilon\nu^5)^{1/4}G_2(\hat{k}/k_s)$ $[\mathrm{s^{-2}\ (cpm)^{-1}}]$

Acknowledgments. The author wishes to thank the Applied Physics Laboratory, University of Washington for their financial assistance and hospitality during a stimulating sabbatical year spent in their laboratory. Mike Gregg, Terry Ewart and Tom Sanford of the Ocean Physics Division deserve special thanks. I would like to acknowledge the special contribution of Greg Holloway who suggested the comparison of potential energy and kinetic energy dissipation and the calculation of Γ.

APPENDIX

Universal Velocity Spectrum

This diversion is included in an effort to present what is commonly referred to as the "Nasmyth Universal Spectrum." It has been presented graphically in a thesis by Nasmyth (1970), but numerical values have been circulated by "personal communication" among those people interested. The formulas are included as a framework for the numerical data presented in Table A1.

The Kolmogoroff description of isotropic turbulence is usually presented in terms of the wavenumber k of the Fourier decomposition of the field. The three-dimensional energy spectral density is defined as

$$\int_0^\infty E(k)dk = \tfrac{1}{2}q^2 = \tfrac{1}{2}(u_1^2 + u_2^2 + u_3^2), \quad \text{(A1)}$$

where u_1, u_2 and u_3 are turbulent velocity components. Experimentally we can only measure a one-dimensional spectrum of the form

$$\int_0^\infty \phi_{11}(k_1)dk_1 = \overline{u_1^2}, \quad \text{(A2)}$$

where $\phi_{11}(k_1)$ represents energy density of the u_1 component with all fluctuations having a wavenumber component k_1 in the x_1 direction. Such a measurement might be made with a heated film moving in the x_1 direction. Alternatively, the spectrum

$$\int_0^\infty \phi_{22}(k_1)dk_1 = \overline{u_2^2}, \quad \text{(A3)}$$

where $\phi_{22}(k_1)$ represents the energy density of the u_2 component of velocity associated with all fluctuations having a wavenumber component k_1 in the x_1 direction. In a locally isotropic wavenumber space (Monin and Yaglom, 1975) one finds that $\phi_{11}(k_1)$ and $\phi_{22}(k_1)$ are related by

$$\phi_{22}(k) = \tfrac{1}{2}\left[\phi_{11}(k_1) - k_1\frac{\partial\phi_{11}(k_1)}{\partial k_1}\right]$$

with units of $[(\text{m s}^{-1})(\text{rad m}^{-1})^{-1}]$. (A4)

It is the spectrum of $\phi_{22}(k_1)$ which is measured by the velocity-shear sensors described in the present study. Dissipation of turbulent kinetic energy is obtained from the measured spectrum of $\phi_{22}(k_1)$ by

$$\epsilon = \frac{15}{2}\nu\int_0^\infty k_1^2\phi_{22}(k_1)dk_1 \quad [\text{m}^2\,\text{s}^{-3}], \quad \text{(A5)}$$

where ν is the kinematic viscosity and ϵ the dissipation per unit mass. At sufficiently high Reynolds numbers the statistical properties of turbulence at small scales are independent of the large-scale flow and depend only on the rate ϵ at which energy is passed from larger to smaller scales, on the kinematic viscosity ν, and on the wavenumber k. A characteristic wavenumber k_s can be defined as

$$k_s = (\epsilon\nu^{-3})^{1/4} \quad [\text{m}^{-1}] \quad \text{(A6)}$$

and dimensional analysis gives

$$\phi_{11}(k_1) = (\epsilon\nu^5)^{1/4}F(k_1/k_s) \quad [(\text{m}^2\,\text{s}^{-2})(\text{rad m}^{-1})^{-1}], \quad \text{(A7)}$$

$$\phi_{22}(k_1) = (\epsilon\nu^5)^{1/4}\tfrac{1}{2}\left[F(k_1/k_s) - k_1\frac{\partial F(k_1/k_s)}{\partial k_1}\right]$$

$$= (\epsilon\nu^5)^{1/4}F_2(k_1/k_s) \quad [(\text{m}^2\,\text{s}^{-2})(\text{rad m}^{-1})^{-1}]. \quad \text{(A8)}$$

Both $F(k/k_s)$ and $F_2(k/k_s)$ are functions of the nondimensional wavenumber k/k_s. In the present study one is concerned with measurements of $\phi_{22}(k_1)$ and considers the "universal" form $F_2(k/k_s)$ derivable from $F(k/k_s)$ (k is used rather than k_1 where no confusion arises).

Velocity shear can be represented as a dissipation spectrum given by

$$k^2\phi_{22}(k) = k_s^2(\epsilon\nu^5)^{1/4}G_2(k/k_s) \quad [\text{s}^{-2}\,(\text{rad m}^{-1})^{-1}], \quad \text{(A9)}$$

where

$$G_2(k/k_s) = (k/k_s)^2F_2(k/k_s), \quad \text{(A10)}$$

which is another "universal" spectral form. Neither $F(k/k_s)$, $F_2(k/k_s)$ or $G_2(k/k_s)$ are represented analytically. The experimentally determined form of Nasmyth (1970; also personal communication) has been used. A summary derived from his spectrum of $F(k/k_s)$ vs k/k_s is given in Table A1. In the analysis of this paper, the cyclic wavenumber $\hat{k}$ has been used rather than the radian wavenumber k, where $\hat{k} = k/2\pi$. This introduces a factor of 2π in the universal forms and, for example, $\phi_{22}(\hat{k})$ is expressed as

$$\phi_{22}(\hat{k}) = k_s^2(\epsilon\nu^5)^{1/4}F_2(\hat{k}/k_s) \quad [(\text{m s}^{-1})^2\,(\text{cpm}^{-1})],$$

where $F_2(\hat{k}/k_s) = 2\pi F_2(k/k_s)$. Table A1 reflects this conversion to cyclic wavenumber, and the computation of $F_2(\hat{k}/k_s)$ from $F(\hat{k}/k_s)$ has been done using Eq. (A8) and a three-point quadratic fit to $\log_{10}F(\hat{k}/k_s)$ versus $\log_{10}(\hat{k}/k_s)$.

REFERENCES

Batchelor, G. K., 1959: Small-scale variation in convected quantities like temperature in a turbulent fluid. *J. Fluid Mech.*, **5**, 113–133.

Caldwell, D. R., T. M. Chriss, P. A. Newberger and T. M. Dillon, 1981: The thinness of oceanic gradients. *J. Geophys. Res.*, **86**, 4290–4292.

——, T. M. Dillon, J. M. Brubaker, P. A. Newberger and C. A. Paulson, 1980: The scaling of vertical gradient spectra. *J. Geophys. Res.*, **85**, 1917–1924.

Dillon, T. M., and D. R. Caldwell, 1980: The Batchelor spectrum and dissipation in the upper ocean. *J. Geophys. Res.*, **85**, 1910–1916.

Fabula, A. G., 1968: The dynamic response of towed thermometers. *J. Fluid Mech.*, **34**, 449–464.

Gibson, C. H., 1968: Finestructure of scalar fields mixed by turbulence, 1, 2. *Phys. Fluids*, **11**, 2305–2327.

Grant, H. L., B. A. Hughes, N. M. Vogel and A. Molliet, 1968: The spectrum of temperature fluctuations in a turbulent flow. *J. Fluid Mech.*, **34**, 423–442.

Lilly, D. K., D. E. Waco and S. I. Adelfang, 1974: Stratospheric

mixing estimated from high-altitude turbulence measurements. *J. Appl. Meteor.*, **13,** 488–493.

Monin, A. S., and A. M. Yaglom, 1975: *Statistical Fluid Mechanics: Mechanics of Turbulence.* Vol. 2, J. L. Lumley, Ed., MIT Press, 874 pp.

Munk, W. J., 1966: Abyssal recipes. *Deep-Sea Res.*, **13,** 707–780.

Nasmyth, P., 1970: Oceanic turbulence. Ph.D. thesis, Institute of Oceanography, University of British Columbia, 69 pp.

Oakey, N. S., 1977: An instrument to measure oceanic turbulence and microstructure. Bedford Institute of Oceanography, Rep. Ser. BI-R-77-3, 52 pp.

——, and J. A. Elliott, 1982: Dissipation within the surface mixed layer. *J. Phys. Oceanogr.*, **14,** 171–185.

Osborn, T. R., 1974: Vertical profiling of velocity microstructure. *J. Phys. Oceanogr.*, **4,** 109–115.

——, 1980: Estimates of the local rate of vertical diffusion from dissipation measurements. *J. Phys. Oceanogr.*, **10,** 83–89.

——, and C. S. Cox, 1972: Oceanic finestructure. *Geophys. Fluid Dyn.*, **3,** 321–345.

——, and W. R. Crawford, 1980: An airfoil probe for measuring velocity fluctuations in the water. *Air-Sea Interaction: Instruments and Methods*, F. W. Dobson, L. Hasse and R. Davis, Eds., Plenum, 369–386.

——, and T. E. Siddon, 1975: Oceanic shear measurements using the airfoil probe. *Proc. Third Biennial Symposium on Turbulence in Liquids*, G. K. Patterson and J. L. Zaken, Eds., University of Missouri-Rolla.

Siddon, T. E., 1971: A miniature turbulence gauge utilizing aerodynamic lift. *Rev. Sci. Instrum.*, **42,** 653–656.

Stewart, R. W., and H. L. Grant, 1962: Determination of the rate of dissipation of turbulent energy near the sea surface in the presence of waves. *J. Geophys. Res.*, **62,** 3177–3180.

Weinstock, J., 1978: Vertical turbulent diffusion in a stably stratified fluid. *J. Atmos. Sci.*, **35,** 1022–1027.

Williams, R. M., and C. A. Paulson, 1977: Microscale temperature and velocity spectra in the atmospheric boundary layer. *J. Fluid Mech.*, **83,** 547–567.